Journal of Applied Polymer Science

Clay Dispersion Effects on Excimer Laser Ablation of Polymer–Clay Nanocomposites

I-Ta Chang, Erol Sancaktar
Department of Polymer Engineering, The University of Akron, Akron, Ohio 44325-0301
Correspondence to: E. Sancaktar (E-mail: erol@uakron.edu)

ABSTRACT: The ablation behavior of polystyrene-organically modified montmorillonite (OMMT) nanocomposites was evaluated by measuring the weight loss induced by KrF excimer laser irradiation of the nanocomposite specimens under air atmosphere. The characteristic values of ablation, ablation threshold fluence, and effective absorption coefficient for polystyrene and its nanocomposites were calculated based on the weight loss data. The effects of morphology due to spatial variation in injection molded samples are also discussed in this article. Results demonstrate that both the dispersion state and the concentration of clay play important roles in excimer laser ablation. The sensitivity of threshold fluence and absorption coefficient to dispersion state of OMMT seem to depend on the clay concentration. © 2013 Wiley Periodicals, Inc. J. Appl. Polym. Sci. 130: 2336–2344, 2013

KEYWORDS: clay; composites; properties and characterization; polystyrene; molding

Received 2 December 2012; accepted 21 April 2013; Published online 22 May 2013
DOI: 10.1002/app.39445

INTRODUCTION

Photo-stability and thermal stability of polymer–clay nanocomposites have been studied by many research groups since they became a popular topic in both industrial and academic fields. The inclusion of clay particles accelerates the photo-oxidation of the polymer–clay nanocomposite, and the photo-oxidation rate increases as the organically modified montmorillonite (OMMT) content increases. Larger *d*-spacing (the distance between similar atomic planes in clay) also results in higher rate of photo-degradation. However, the degree of clay dispersion has little influence on the photo-oxidative degradation of the polymer matrix.[1–6] The thermal-oxidation stability of polymer–clay nanocomposites is improved compared with the pure polymer matrix and is enhanced with increasing clay concentration. Higher intercalation and dispersion states of OMMT also increase the thermal stability of the nanocomposites.[7–10]

UV excimer laser ablation of polymers can be considered an extreme condition for photo-degradation of polymers due to high power output in very short pulse width (~25 ns) provided by the excimer laser.[11] Excimer laser ablation removes layers from polymer surfaces with very little thermal damage to the bulk.[11,12] Two mechanisms, photo-thermal and photo-chemical, have been considered for excimer laser ablation on polymers. Many scientists found that these two mechanisms could take place simultaneously depending on the nature of the polymers and the processing conditions.[13–15] Generally speaking, when a polymer is ablated by excimer laser in atmospheric environment, oxidation can be initiated through photo-thermal and photo-chemical reactions, and leads to the degradation or decomposition of the polymer.[12] Therefore, the photo and thermal stability of the material may need to be taken in to account. The excimer laser ablation of polymer–clay nanocomposites is a complex topic due to the variety of parameters and very limited literatures. The intention of this article was to investigate the ablation behavior of polystyrene (PS)–OMMT nanocomposites with various clay contents and melt-compounding times by measuring the ablation weight loss.

EXPERIMENTAL

Materials

The polymer used in this study was Styron 615APR general purpose polystyrene pellets (Dow Chemical, Midland, MI). The OMMT chosen for this study was Cloisite 20A, donated by Southern Clay Products (Gonzales, TX). Cloisite 20A is a natural MMT modified with dimethyl dehydrogenated tallow quaternary ammonium salt with d_{001} of 2.42 nm. All materials were dried in a vacuum oven at 80°C for 24 h. Table I lists the compositions of the nanocomposites used in this research.

Sample Preparation

Melt Blending. The PS–OMMT nanocomposites were prepared by melt blending the dry-mixed PS/clay mixtures in a Mini Twin-Screw Co-rotation Compounder equipped with recirculation channel (HAAKE Mini Lab CTW5, Madison, WI) at 150°C and 120 rpm for 2–10 min. The mixing chamber was filled with

Table I. Compositions of PS–Clay Nanocomposites Used in this Research

PS	100	0
PSNC01	99	1
PSNC03	97	3
PSNC05	95	5
PSNC10	90	10

nitrogen gas to avoid degradation of materials during the process. Neat-polystyrene control samples were also prepared in identical conditions.

Injection Molding. The pulverized samples were injection-molded into rectangular shaped specimens by a Mini Injection Molding Machine (DSM, Geleen, The Netherlands) using 170°C barrel temperature and 30°C mold temperature. Figure 1 shows the dimensions of the specimen. The injection force was 4.5 N. The rectangular bar samples were cut into several pieces along the flow direction using a diamond-cutting saw for the subsequent excimer laser ablation test.

X-ray Diffraction (XRD)

XRD analyses and PS–clay nanocomposites were performed on a Rigaku (Woodlands, TX) diffractometer using Cu $K\alpha$ radiation with wavelength of 0.15418 nm. The scanning range (2θ) was 1.5∼10° at the rate of 0.015 degrees/s under reflective mode. The XRD patterns were obtained from sectioned pieces of predetermined positions on the rectangular bars as shown in Figure 2.

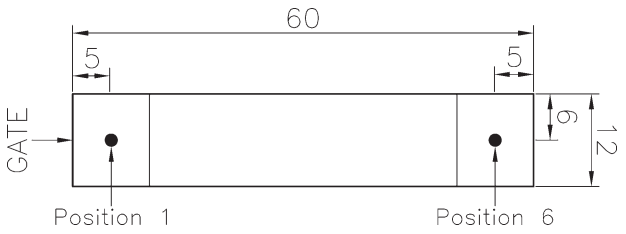

Figure 1. Ablation position of the injection-molded specimens (unit: mm).

The 2D XRD pattern of clay were collected by a Bruker AXS (Madison, WI) D8 Discover X-ray diffractometer operated in transmission mode with measuring periods of 30 s at room temperature and the goniometer was set at $\chi = 45°$. The background scattering resulted from the scotch tape on empty sample holder was subtracted from the experimental curves. The 2D XRD data were obtained from both B-cut slice (FD-ND plane) in the center and C-cut slice (FD-TD plane) of sample surface at 250–350 μm slice thickness. Figure 2 shows the cutting procedure. The X-ray beam was directed along the transverse direction at the skin region of B-cut slices and along the normal (thickness) direction at center of C-cut slices.

Excimer Laser Ablation

A Lambda Physik (Göttingen, Germany) excimer laser (LPX 240i) was used to ablate samples at 248 nm wavelength (KrF) with pulse duration of 25 ns. Sample surfaces were kept perpendicular to the direction of the laser beam. The laser beam was masked to a circular shape of 1.6 mm diameter using a steel mask and a venting tube connected to a vacuum pump was placed on the mask to evacuate the debris to prevent them from re-depositing on the ablated surface. All samples were ablated at two predetermined positions using 500 pulses at 1 Hz and at four laser fluencies varying from 300 to 1000 mJ/cm^2. Figure 2 shows the ablation positions of the injection-molded specimens.

Weight Loss Measurement

The measurement of the sample weight loss induced by excimer laser ablation is a practical and accurate way to evaluate the ablation behavior. The sample weight is measured and recorded before and after ablation by using a Mettler Toledo (Columbus, OH) AX205 analytical balance with an accuracy of 0.01 mg. The weight loss data is obtained as the average of three or four replicated laser ablation experiments. By plotting ablation depth

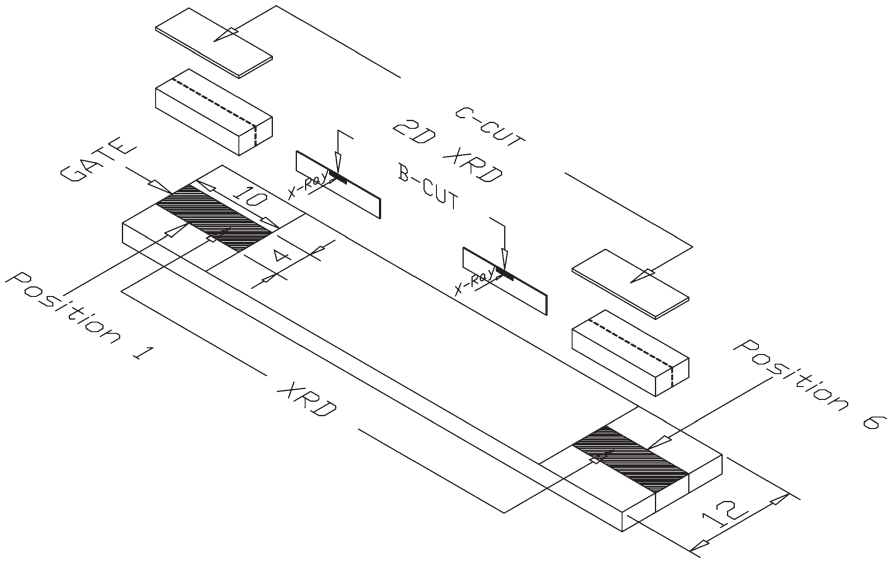

Figure 2. Schematic of the specimen sections used for XRD measurements (unit: mm).

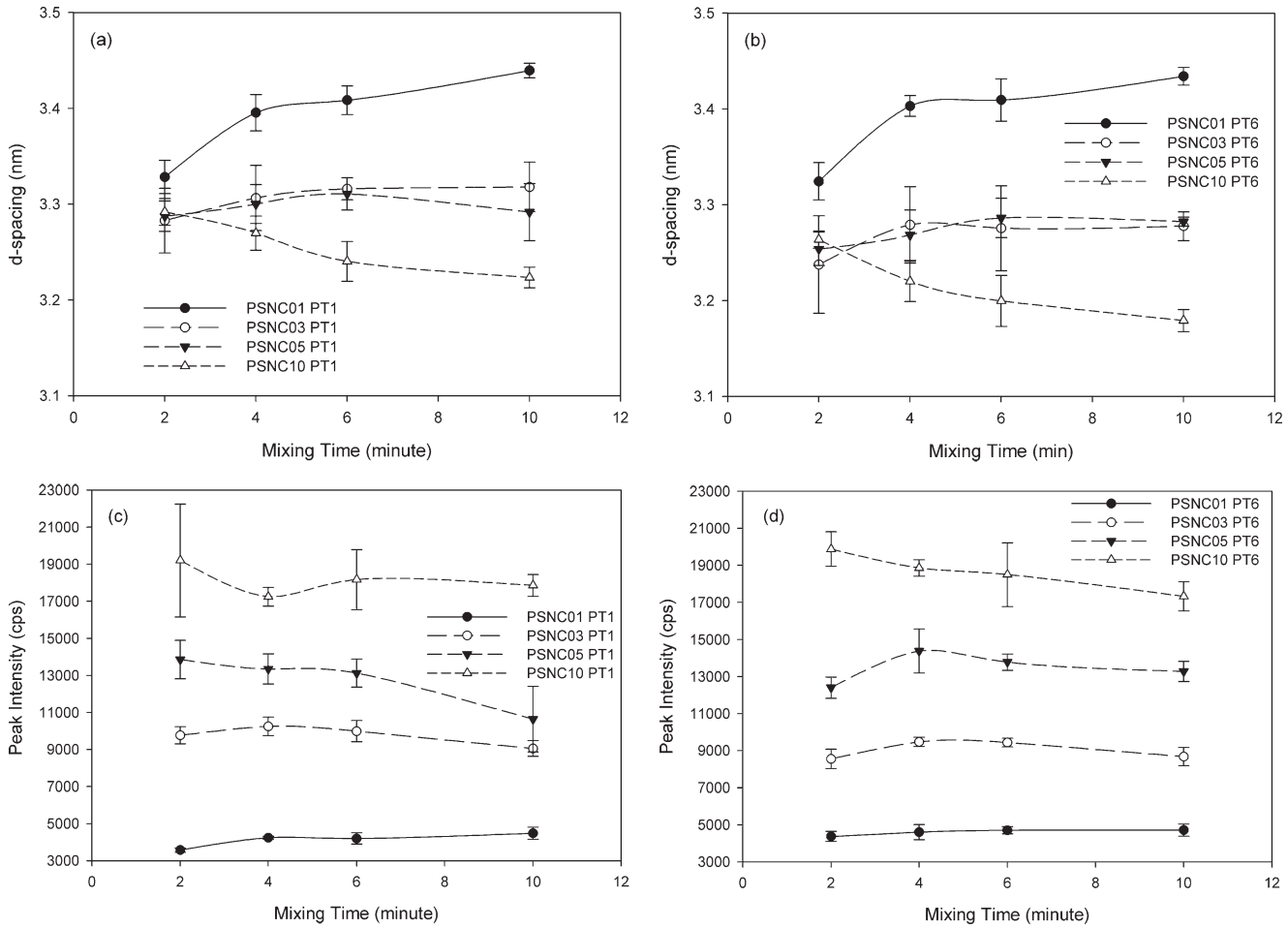

Figure 3. The effects of mixing time on XRD for PS-clay nanocomposites as measured at two positions (PT1 and PT6).

per pulse (derived form weight loss) with respect to incident laser fluence and fitting the curve with Beer's law, threshold fluence and effective absorption coefficients of samples were calculated.

RESULTS AND DISCUSSION

XRD Results

Figure 3 shows the effects of mixing time on XRD for PS–clay nanocomposites at both positions. All the nanocomposite samples in this study showed an increase of gallery height ranging from 3.179 to 3.439 nm compared to 2.35 nm for the pristine OMMT, indicating that good compatibility exists between polystyrene molecules and the organically modified clay we used.[6] However, our XRD results also revealed that none of the samples achieved full exfoliation of the clay layers, which would have been revealed by the absence of a diffraction peak in XRD spectra.

It is very clear that interlayer spacing-mixing time curves were heavily affected by OMMT concentration and can be divided into three groups: (1) *d*-spacing increased steadily with increased mixing time for dilute system containing 1 wt % of clay; (2) d_{001} increased by very small amount or kept constant for samples having moderate concentration, 3–5 wt %, and (3) *d*-spacing decreased for high clay loading (10 wt %) composites. For both positions, the *d*-spacing decreased with an increase of clay loading and gaps widened with increased mixing time (except 10%). High content of OMMT in polymer matrix not only results in non-uniform dispersion and agglomeration of clay layers, but also reduces the mobility of polymer chains, and consequently restrains the polymer from penetrating into the clay gallery.[16] As a result, PSNC10 exhibited the smallest *d*-spacing. Therefore, we can reach a conclusion that there is a limit of about 5 wt % for the OMMT concentration for melt compounding of polymer–clay nanocomposites to achieve good expansion of interlayer spacing. Tanoue et al.[17] also reported a similar conclusion on melt compounding of different grades of polystyrene with organoclay using a twin-screw extruder.[17]

Although the location shows very little effect on the shape of *d*-spacing-mixing time curves, it is worth noting that only the *d*-spacing of PSNC01 was not affected by location, while other samples containing higher OMMT loadings all showed higher *d*-spacings at position 1 than those at position 6. This behavior stems from more compacted arrangement at position 6 caused by additional shear and elongation processes,[18] and therefore, with increased face to face collision between particles due to reduced inter-particle distance at higher clay concentration, the

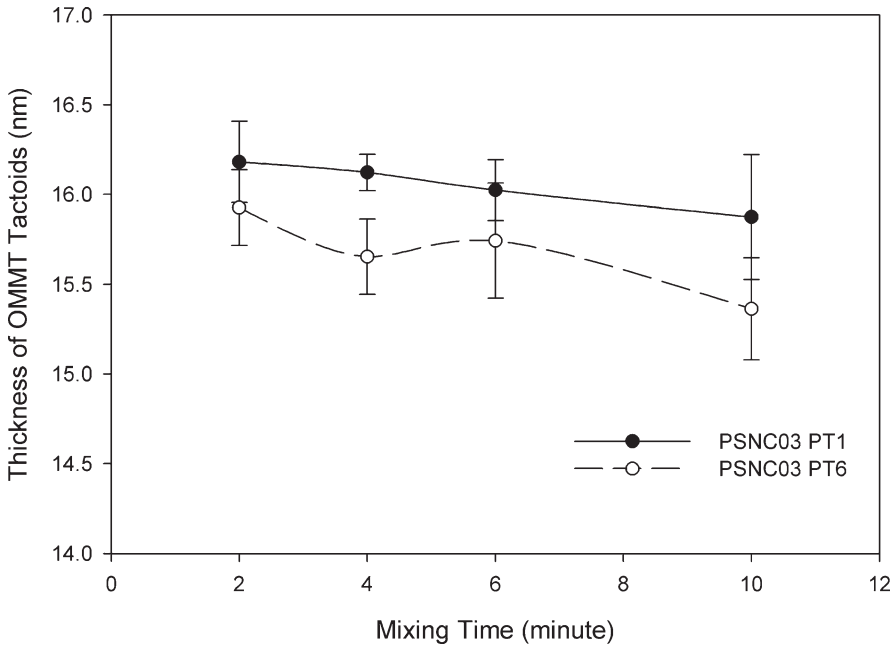

Figure 4. The effects of mixing time on the thickness of clay tactoid for 3 wt % clay loading in PS (PSNC03) at two positions (PT1 and PT6).

clay particles were compressed during injection molding reducing the *d*-spacing.

The impact of clay content on peak intensity-mixing time curves can also be observed on Figure 3(c,d). These curves evolve from simply increasing with mixing time (indicating more clay platelets parallel to specimen surface and increasing of intercalation7) at 1 wt % clay concentration to concave-down shape (increasing first then decreasing), to simply decreasing and to almost flat line (position1 of PSNC10) as the OMMT concentration increased. In addition, the decrease of peak width (FWHM) with mixing time can only be observed with PSNC01 samples, while other samples exhibit an increasing behavior. The change in curve shape is due to delamination and partial exfoliation of OMMT platelets which took place in higher clay weight fraction (3–10 wt %) samples due to their higher viscosities and resulted in reduced peak intensity. Using the Scherrer equation, the thickness of the OMMT tactoid can be estimated as following:

$$t = \frac{K \times \lambda}{\beta \cos \theta}, \quad (1)$$

where t is thickness, K is constant dependent on crystallite shape (0.9), λ is wavelength of X-ray, β is FWHM (full width at half maximum), and θ is Bragg Angle.[7] Figure 4 shows that the thickness of tactoid decreased with the mixing time at both positions (16.18–15.87 at PT1 and 15.93–15.36 nm at PT6) for PSNC03 samples.

The intensity of diffraction peak was also heavily affected by clay concentration. The intensity values increased dramatically with the OMMT weight fraction, and this increase was not linearly proportional to clay loading. This nonlinear relationship can be attributed to the different degrees of exfoliation exhibited at different clay contents. Tanoue et al.[17] also suggested that if the extent of exfoliation is enhanced with the OMMT loading, the gradient of this effect will be reduced, and vice versa.

It is also interesting to note that the tendency of peak intensity-mixing time curves were affected by the position for the composites containing higher amount of clay (5 and 10 wt %). This is the consequence of some dispersed/delaminated OMMT platelets being able to maintain their structural regularity due to the combined effects of compacted/orientated arrangement at point 6 and high clay concentration. Therefore, the clay weight fraction of 5% can be considered to be the threshold value for this kind of behavior.

2D XRD patterns of 4 min-mixed PSNC03 sample are shown in Figure 5. It can be seen clearly that no peak was visible from FD-TD (C-cut) slice and a strong peak signal appears at $2\theta \approx 2.67$ for PT1 (2.70 for PT6). This result reveals that the OMMT tactoids were orientated along the flow direction and their surfaces were parallel to the normal (thickness) direction of the injection molded samples.[18,19] The average orientation function of clay platelets (S) can be calculated from the 2D XRD data using the following equation:

$$S = \frac{-2\int_0^{\pi/2} I(\chi)P(\chi)\sin(\chi)d\chi}{\int_0^{\pi/2} I(\chi)\sin(\chi)d\chi} \quad \text{and} \quad P(\chi) = \frac{3(\cos^2\chi)-1}{2}, \quad (2)$$

where $I(\chi)$ is the intensity at azimuthal angle χ.[18] The result,-shown in Figure 6, indicated that the orientation function increased with mixing time and position 6 exhibited higher value of orientation function than position 1.

Ablation Weight Loss

The effects of mixing time on laser ablation weight loss at fluence of 500 mJ/cm^2 for PS/OMMT nanocomposites are shown in Figure 7. For neat-polystyrene samples, the mixing time has little influence on the ablation weight loss at

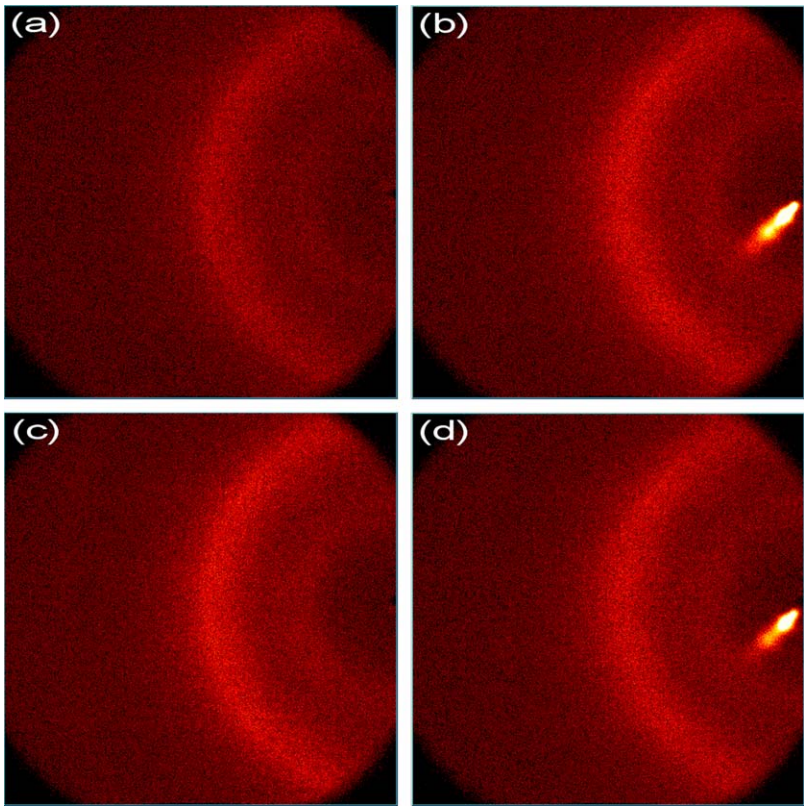

Figure 5. 2D XRD patterns for 4 min mixed 3 wt % clay loading in PS (PSNC03) at two positions. (a) PT1-ND, (b) PT1-TD, (c) PT6-ND, and (d) PT6-TD. [Color figure can be viewed in the online issue, which is available at wileyonlinelibrary.com.]

both positions [Figure 7(a)], while position 1 (near the gate) exhibits higher weight loss than position 6 (near the end). This position effect was first reported by Sancaktar et al.[20] and can be attributed to the high degree of orientation of polymer molecules along the injection direction at the position near the end of sample resulting in a more compact arrangement, which is more difficult to ablate.

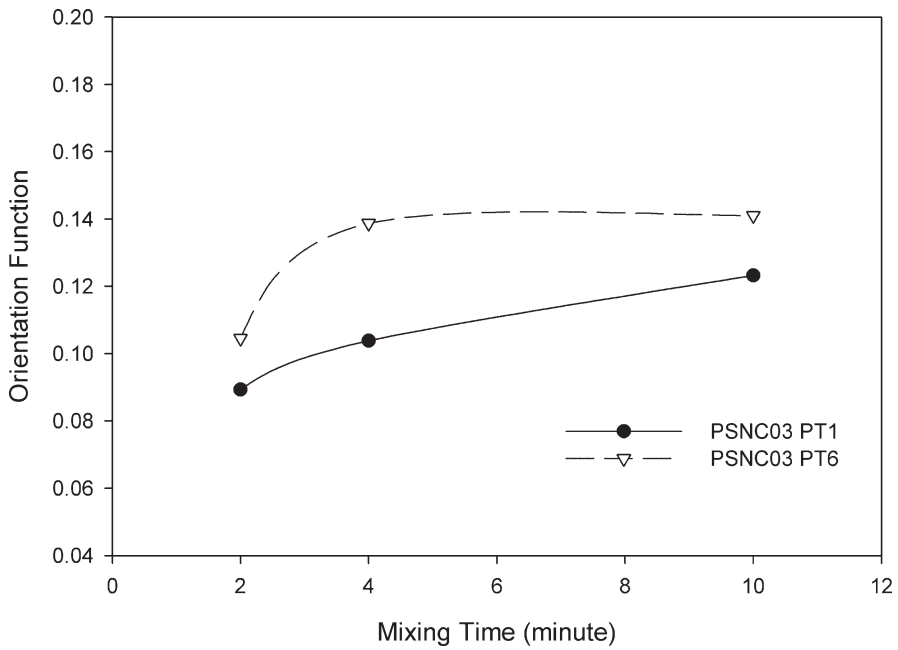

Figure 6. The effects of mixing time on the orientation factor of clay tactoid for PSNC03 at two positions (PT1 and PT6).

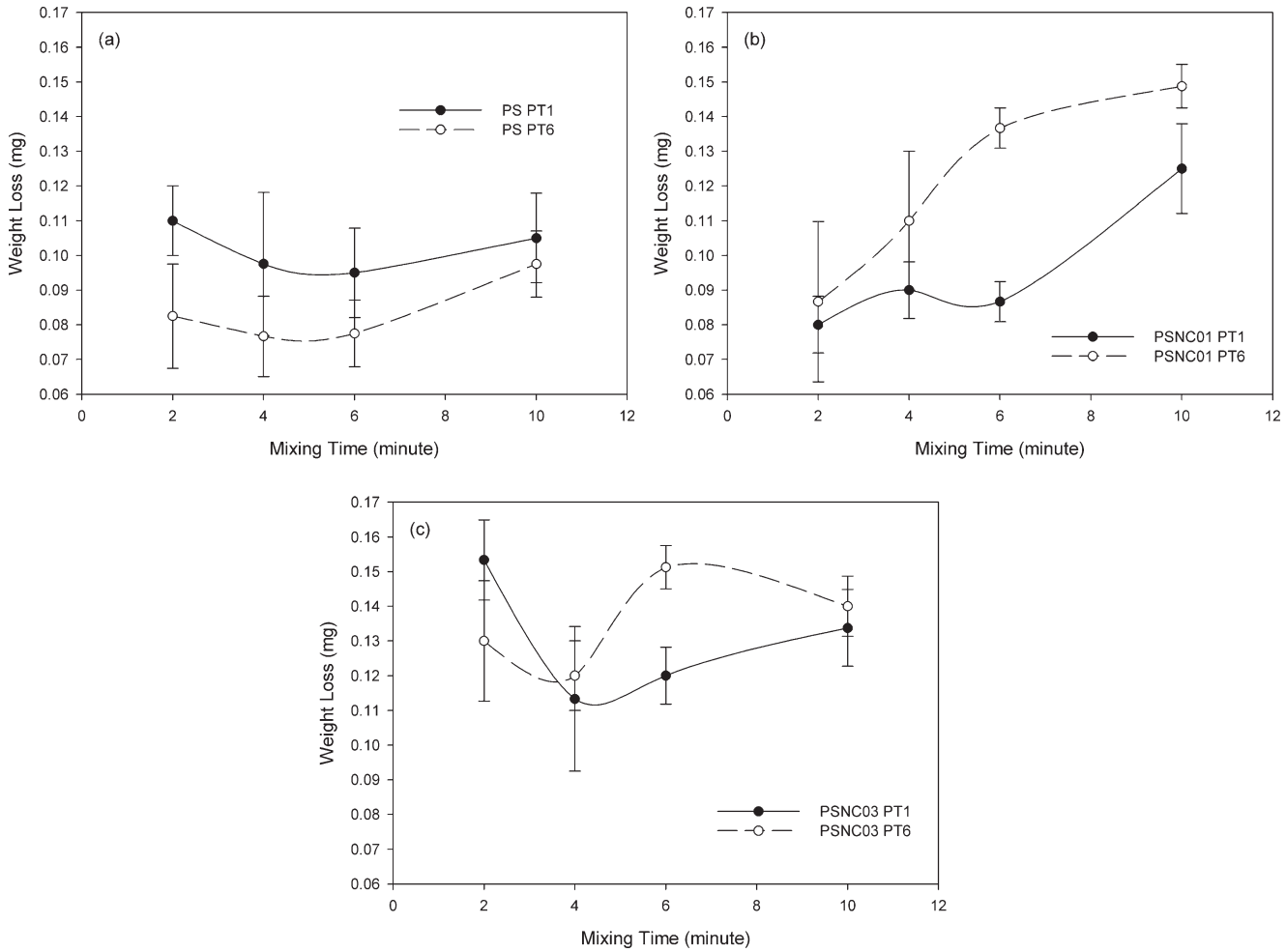

Figure 7. The effects of mixing time on ablation weight loss for PS–clay nanocomposites as measured at two positions (PT1 and PT6) for: (a) homogeneous PS, (b) 1 wt % clay loading in PS (PSNC01), and (c) 3 wt % clay loading in PS (PSNC03).

Figure 7(b) and (c) reveals that, contrary to what is observed with homogeneous PS, when the nanoclay is added at 1 and 3 wt % levels, position 6 exhibits higher ablation weight loss than position 1 at all mixing times except at 2 min mixing for PSNC03 [Figure 3(b,c)].

Figure 7(b) illustrates that when the mixing time was increased for PSNC01, the ablation weight loss at both positions increased from 0.080 to 0.1250 mg by 56.3% and 0.0867 to 0.1487 mg by 71.6% for positions 1 and 6, respectively. For the 1 wt % nanocomposite samples, position 6 shows higher peak intensity than position 1 at all four mixing times, higher reflected energy indicating higher dispersion. The increasing weight loss can be attributed to the increase in clay platelets parallel to specimen surface with increasing mixing time. When clay platelets are parallel to specimen surface (specific surface area of MMT is A_{sp} = 750∼800 m^2/g^7), they provide the maximum surface to be irradiated by the excimer laser which is perpendicular to the sample surface. Compared with polystyrene, the MMT has much higher absorption coefficient at λ = 248 nm (2.08–2.47 vs. 0.65 cm^{-1}) and much lower specific heat (0.7996 vs. 1.647 J/g·°C).[21–24] Therefore, more UV energy can be absorbed, and clay platelets are heated more efficiently resulting in accelerated photo-thermal ablation on PS chains. With increased number of clay platelets parallel to the specimen surface, more hot spots will be generated under UV irradiation, and consequently, more clay induced photo-thermal ablation will take place. Position 6 shows higher ablation weight loss due to more clay particles being parallel to the specimen surface (indicated by our XRD data), leading to enhanced clay induced photo-thermal ablation on PS chains.

For PSNC03 samples, weight loss decreases when mixing time is increased from 2 to 4 min (0.1533 to 0.1133 mg and 0.1300 to 0.1275 mg for positions 1 and 6, respectively), and then increases (0.1133 to 0.13380 mg and 0.1275 to 0.140 mg for positions 1 and 6, respectively) when the mixing time is increased from 4 to 10 min. Position 6 shows higher ablation weight loss than position 1 except at 2 min mixing time. For both positions, the 2 min mixing time must result in a system containing larger sizes of clay particles with high stacks of clay platelets which absorb more laser energy due to their larger thickness; thus, more laser energy is transferred into the surrounding polystyrene molecules enhancing clay induced photo-thermal ablation on PS chains and resulting in higher ablated weight loss at 2 min mixing time than at 4 min, with this effect

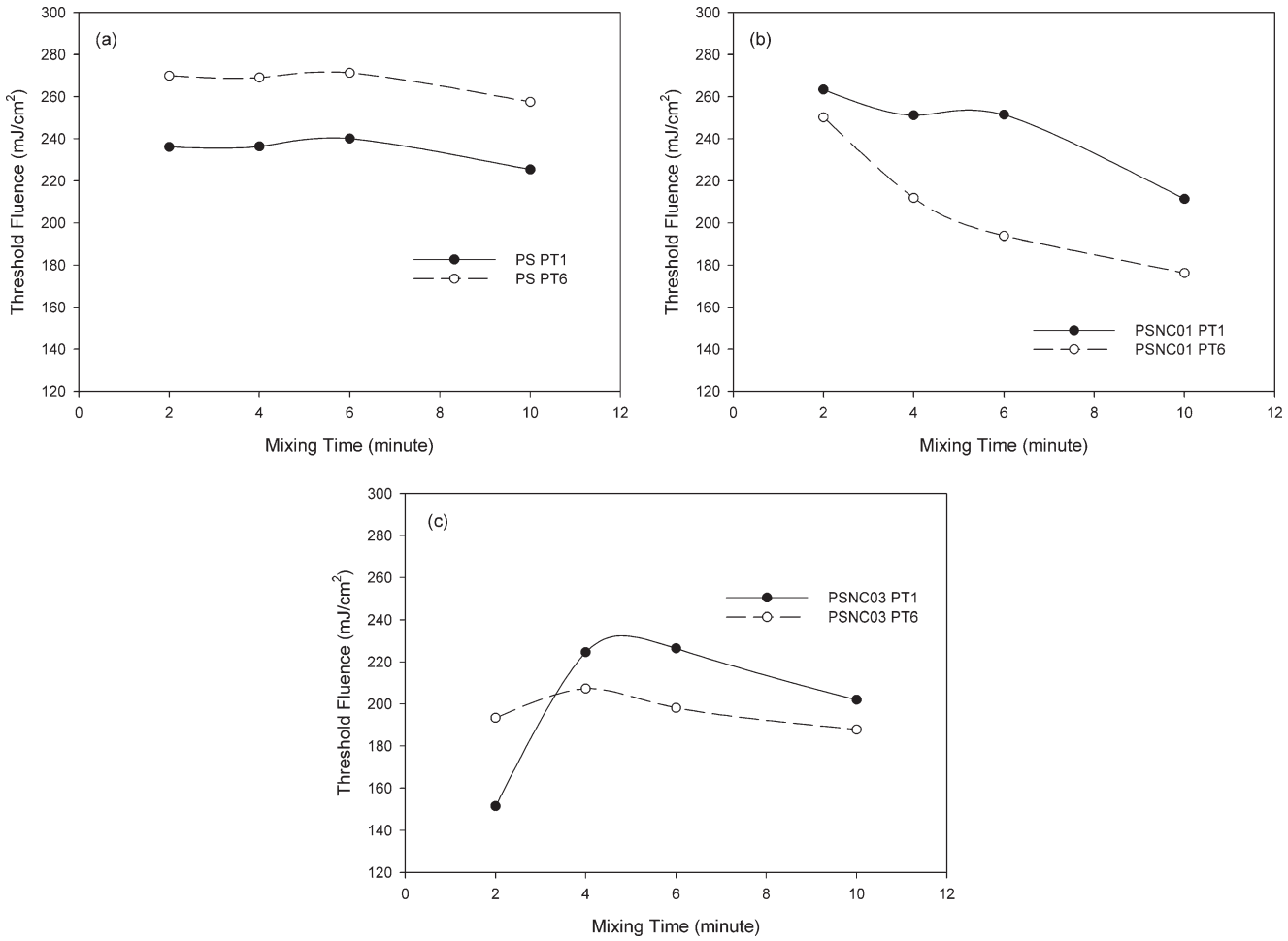

Figure 8. The effects of mixing time on threshold fluence for PS-clay nanocomposites as measured at two positions (PT1 and PT6) for: (a) homogeneous PS, (b) 1 wt % clay loading in PS (PSNC01), and (c) 3 wt% clay loading in PS (PSNC03).

being stronger at position 1 than at position 6. For this particular case, perhaps clay stacks breakage occurs as the stacks travel down to position 6. As the number of clay layers reduces when the OMMT particles break into thinner pieces and exfoliation of some platelets takes place at longer mixing time, the absorption of laser energy by single PS–clay domain is also reduced leading to less heat transfer and decreased weight loss. However, better dispersion/intercalation/exfoliation of OMMT particles at 6 and 10 min mixing times result in not only greater surface area of clay platelets to absorb the laser energy but also in increased number of PS–clay domains. Consequently, more "hot spots" are generated leading to the increase in weight loss.

We note that laser induced amorphization of OMMT may occur under certain conditions as reported in Ref. [25]. No investigation was performed in this current work on whether such amorphization has occurred in our system.

Ablation Threshold Fluence and Absorption Coefficient

The ablation depth per pulse, X, can be approximated from ablation weight loss due to multiple laser pulses using the equation,

$$X = \frac{W}{A\rho n} \tag{3}$$

where, W is ablation weight loss, A is ablation area, ρ is density of materials, and n is number of pulses.[21] The ablation threshold fluence, F_{th}, and effective absorption coefficient, α_{eff}, can be obtained by fitting the ablation depth per pulse (X) versus laser fluence (F_0) curves using Beer's Law:

$$X = \frac{1}{\alpha_{eff}} \ln\left(\frac{F_0}{F_{th}}\right) \tag{4}$$

The effective absorption coefficient, α_{eff}, calculated using this method may be different from the low-signal absorption coefficient, α, of the polymer determined by UV absorption spectroscopy from its transmission behavior under low irradiance fluence and it also has been reported that α_{eff} could be an order magnitude higher than α.[26–28]

The effects of mixing time on threshold fluence and effective absorption coefficients for PS–clay nanocomposites are shown in Figures 8 and 9, respectively. For PS, the higher ablation weight loss behavior at position 1 in comparison to position 6

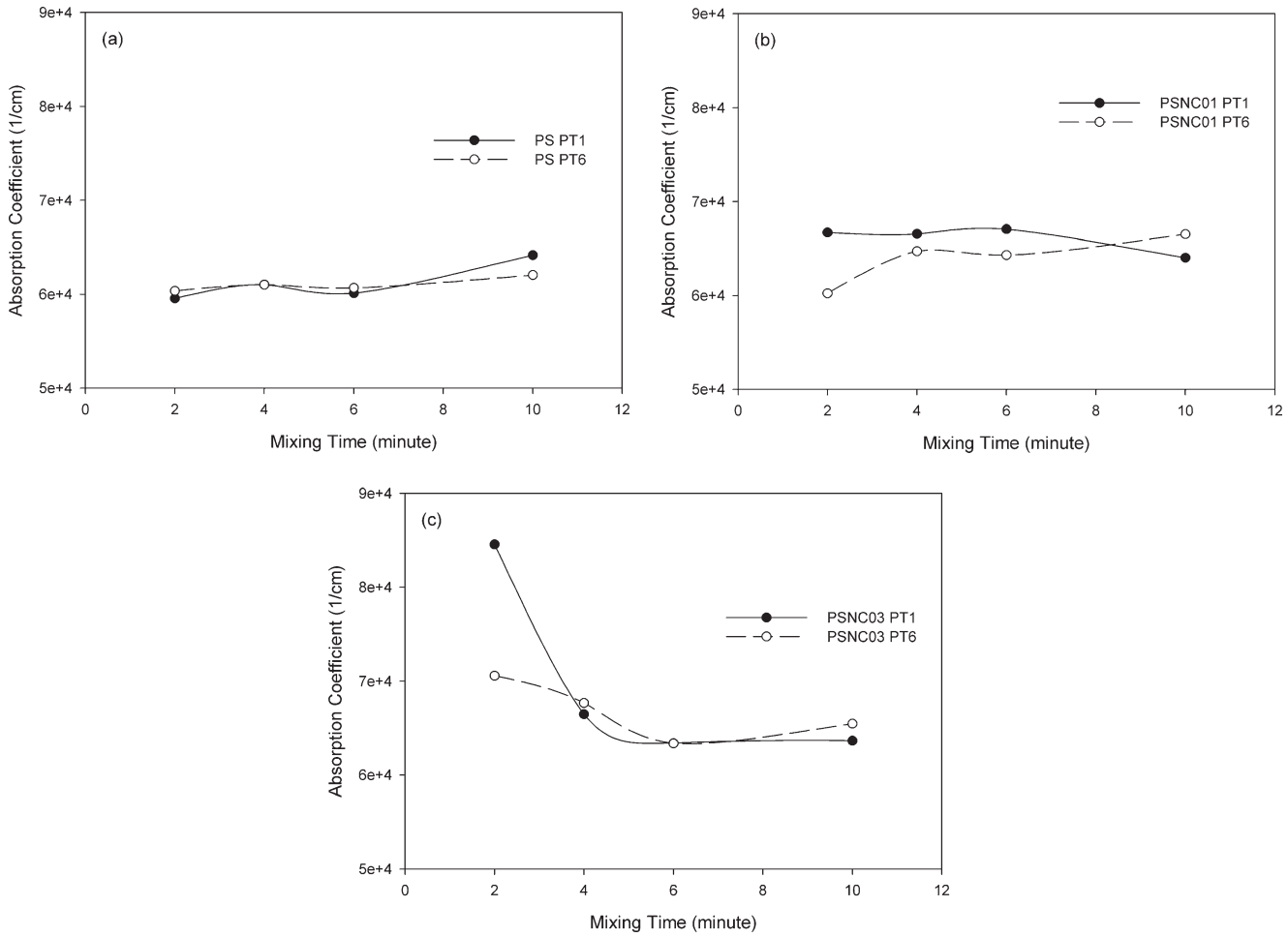

Figure 9. The effects of mixing time on effective absorption coefficients for PS–clay nanocomposites as measured at two positions (PT1 and PT6) for: (a) homogeneous PS, (b) 1 wt % clay loading in PS (PSNC01), and (c) 3 wt % clay loading in PS (PSNC03).

is apparently dominated by the position 1 having lower ablation threshold fluence [Figure 8(a)] rather than higher absorption coefficient [Figure 9(a)] noting that there was no change in chromophore structure within the system. For the case of PSNC01, the observed behavior of increasing ablation weight loss with increasing mixing time at position 1 [Figure 7(b)] apparently relates to the observed behavior of decreasing ablation threshold fluence with increasing mixing time [Figure 8(b)]. Position 6 also shows decreasing of ablation threshold fluence [Figure 8(b)] as well as moderately increasing of absorption coefficient with mixing time [Figure 9(b)]. In comparison to position 1, position 6 exhibits lower values of threshold fluence at all mixing times for PSNC01. The weight loss-mixing time relationships of PSNC03 [Figure 7(c)] more-or-less reflect the behavior observed with the threshold fluence [Figure 8(c)], especially for the changes observed between the 2 and 4 min mixing times, discussed in previous section. Similar change is also observed with the variations in absorption coefficient between 2 and 4 min mixing times [Figure 9(c)]. For the case of PSNC03, both the threshold fluence and absorption coefficient values are less affected by mixing time at position 6 in comparison to position 1.

CONCLUSIONS

The ablation behavior of PS–OMMT nanocomposites was studied via ablation weight loss related to different dispersion/intercalation states resulting from various clay contents and mixing times. It was found that dispersion states-mixing time relationships were heavily affected by the OMMT weight fraction. In general, higher degree of dispersion/intercalation may lead to the increasing of weight loss especially for the low clay loading samples. The sensitivity of threshold fluence and absorption coefficient to dispersion state of OMMT seem to increase with clay concentration.

REFERENCES

1. Pandey, J.; Reddy, K.; Kumar, A.; Singh, R. *Polym. Degrad. Stab.* **2005**, *88*, 234.
2. Wang, J.; Du, J.; Zhu, J.; Wilkie, C. *Polym. Degrad. Stab.* **2002**, *77*, 249.
3. Qin, H.; Zhang, S.; Zhao, C.; Huand G.; Yang. M. *Polymer* **2005**, *46*, 8386.

4. Sloan, J. M.; Patterson, P. Mechanisms of photo degradation for layered silicate-polycarbonate nanocomposites. Report of US Army Research Laboratory, **2005**.
5. Deng, Y.; Gu, A.; Fang, Z. *Polym. Int.* **2004**, *53*, 85.
6. Remili, C.; Kaci, M.; Kachbi, S.; Bruzaud S.; Grohens. Y. *J. Appl. Polym. Sci.* **2009**, *112*, 2868.
7. Utracki, L. Clay-Containing Polymeric Nanocomposite; Rapra Technology Limited: Shawbury, **2004**; Vol. *1*.
8. Vyazovkin, S.; Dranca, I.; Fan X.; Advincula. R. Macromol. . *Rapid. Commun.* **2004**, *25*, 498.
9. Zhang, J.; Jiang, D.; Wilkie. C. *Polym. Degrad. Stab.* **2006**, *91*, 358.
10. Qin, H.; Zhang, S.; Zhao, C.; Feng, M.; Yang, M.; Shu, Z.; Yang, S. *Polym. Degrad. Stab.* **2004**, *85*, 807.
11. Rabek, J. In Photodegradation of Polymers: Mechanisms and Experimental Methods; Springer: New York, **1994**.
12. Duley, W. UV Lasers: Effects and Applications in Materials Science; Cambridge University Press: Cambridge, **1996**.
13. Ozdemir, M.; Sadikoglu, H. *Trends Food Sci. Technol.* **1998**, *9*, 159.
14. Srinivasan, R. In Laser Ablation: Principles and Applications; Miller, J. C., Eds.; Springer: New York, **1994**; pp 107–133.
15. Feng, Y.; Liu, Z. Q.; Yi, X.-S. *Appl. Surf. Sci.* **2000**, *156*, 177.
16. Lew, C. Y.; Murphy, W. R.; McNally, G. M. *Poly. Eng. Sci.* **2004**, *44*, 1027.
17. Tanoue, S.; Utracki, L.; Garcia-Rejon, A.; Tatibouët, J.; Cole, K.; Kamal, M. *Poly. Eng. Sci.* **2004**, *44*, 1046.
18. Galgali, G.; Aagarwal, S.; Lele, A. *Polymer* **2004**, *45*, 6059.
19. Yalcin, B.; Cakmak, M. *Polymer* **2004**, *45*, 6623.
20. Sancaktar, E.; Negandhi, N.; Adwani, S. *J. Appl. Polym. Sci.* **2006**, *101*, 258.
21. Sancaktar, E.; Lu, H. *J. Appl. Polym. Sci.* **2006**, *99*, 1024.
22. Markle, J.; Schincariol, R.; Sass, J.; Molson, J. *Soil Sci. Soc. Am. J.* **2006**, *70*, 1281.
23. Rothe, E. W.; Baird, R. J.; Manke C. W.; Piparia, R. *Nanotechnology*, **2008**, *19*, 165301.
24. Arakawa, E. T.; Tuminello, P. S.; Khare, B. N.; Millham, M. E.; Authier, S.; Pierce, J. In Proceedings of Scientific Conference on Obscuration and Aerosol Research. Aberdeen Proving Ground, June, **1997**.
25. Duchek, P.; Urbanova, M.; Pokorna, D.; Kupcik, J.; Subrt, J.; Pola, J. *J. Non-Cryst. Solids* **2012**, *358*, 3382.
26. Dyer, P. E. *Appl. Phys. A* **2003**, *77*, 167.
27. Skordoulis, C. D.; Makropoulou, M.; Serafetinides, A. A. *Appl. Surf. Sci.* **1995**, *86*, 239.
28. Sancaktar, E.; Lipshitz, H.; Babu, S. V.; Zhang, E.; D'Couto, G. C. *J. Adhes.* **1995**, *50*, 103.